

IMMUNOLOGY

Expression of inhibitory receptors by B cells in chronic human infectious diseases restricts responses to membrane-associated antigens

Abhijit A. Ambegaonkar, Kihyuck Kwak, Haewon Sohn, Javier Manzella-Lapeira, Joseph Brzostowski, Susan K. Pierce*

Chronic human infectious diseases, including malaria, are associated with a large expansion of a phenotypically and transcriptionally distinct subpopulation of B cells distinguished by their high expression of a variety of inhibitory receptors including Fc γ RIIB. Because these B cells, termed atypical memory B cells (MBCs), are unable to respond to soluble antigens, it was suggested that they contributed to the poor acquisition of immunity in chronic infections. Here, we show that the high expression of Fc γ RIIB restricts atypical MBC responses to membrane-associated antigens that function to actively exclude Fc γ RIIB from the B cell immune synapse and include the co-receptor CD19, allowing B cell antigen receptor signaling and differentiation toward plasma cells. Thus, chronic infectious diseases result in the expansion of B cells that robustly respond to antigens that associate with cell surfaces, such as antigens in immune complexes, but are unable to respond to fully soluble antigens, such as self-antigens.

INTRODUCTION

Malaria is a mosquito-borne infectious disease caused by parasites of *Plasmodium* spp. that takes the lives of more than 400,000 individuals each year in Africa alone, mostly among young children (1). Antibodies play a central role in immunity to malaria; however, the acquisition of long-lived protective antibodies in children born in malaria-endemic Africa is extraordinarily slow, requiring years of repeated parasite exposure (2, 3). Children in malaria-endemic areas acquire malaria-specific antibodies and memory B cells (MBCs) in a stepwise fashion so that by their early teens, most children are resistant to febrile malaria (4) but remain susceptible to infection throughout their adult lives (5). At the same time that children gradually acquire protective antibodies and MBCs, they experience a large expansion of a population of B cells that we have termed atypical MBCs. In high malaria-endemic areas, atypical MBCs can represent more than 40% of a child's peripheral blood B cells (6).

Phenotypically and transcriptionally atypical MBCs in malaria are distinct from naïve B cells and classical MBCs (7). In malaria, atypical MBCs lack the classical MBC markers CD21 and CD27 and are CD10⁻, CD19^{Hi}, CD20^{Hi}, and FcRL5^{Hi}. They also express high levels of the T helper 1 transcription factor T-bet and the integrin CD11c. A particularly notable feature of atypical MBCs is their high expression of a variety of inhibitory receptors including Fc γ RIIB, Siglec-6, CD22, CD72, LAIR1, CD85j, and PD-1. We first named these cells atypical MBCs in 2009 (6) selecting the term “atypical” so as not to imply a function for these B cells and “MBCs” to recognize their similarity to the distinctive tissue-based population of human MBCs (CD27⁻ CD21^{Lo} FcRL4⁺) described by Cooper and colleagues (8) in healthy individuals and the subsequent description of tissue-like MBCs (CD27⁻ CD21^{Lo} FcRL4⁺) by Moir and colleagues (9) in HIV-infected high viremic individuals. However, it has become increasingly clear that B cells that phenotypically

and functionally resemble atypical MBCs are expanded in several other chronic infectious diseases including those caused by hepatitis C virus and *Mycobacterium tuberculosis* (10) and in autoimmune diseases in particular in systemic lupus erythematosus (SLE). T-bet⁺ B cells that are CD27 and immunoglobulin D (IgD) double negative (DN) in SLE share several features with malaria-associated atypical MBCs, including elevated expression of T-bet, CD11c, CD95, and CD86 and the inhibitory receptors FcRL5, Fc γ RIIB, and CD22 as well as loss of CD21 and CD27 (11–17). These DN B cells differentiate from activated naïve B cells in extra-follicular sites (15–17) and are enriched in autoreactive specificities (11, 15, 17). However, malaria-associated atypical MBCs do not secrete antibodies directly *ex vivo* even from children during acute malaria infections or in response to combinations of Toll-like receptor (TLR) ligands, cytokines, and B cell receptor (BCR) cross-linking *in vitro* (18). DN B cells in patients with SLE show up-regulation of transcription factor interferon regulatory factor 4 (IRF4) *ex vivo* (13, 15), are poised to become antibody-secreting cells in response to TLR7 ligands and the cytokines interferon- γ and interleukin-21 (IL-21) (15), and are considered to be the direct source of antibody-secreting cells and serum autoantibodies during SLE flares (11, 14, 15, 17).

We reported earlier that atypical MBCs in malaria distinguished themselves by their hyporesponsiveness to BCR stimulation by soluble anti-Ig cross-linking and their failure to differentiate into antibody-secreting plasma cells (PCs) when cultured under conditions sufficient to induce classical MBCs to secrete antibodies (18). In contrast to classical MBCs, atypical MBCs also failed to secrete cytokines when incubated with anti-Ig, anti-CD40, and CpG (18). Similar refractoriness to stimulation by soluble antigen has been reported for atypical MBCs in other chronic infectious diseases including AIDS (9). It has been suggested that atypical MBCs are “exhausted” in analogy to T cell exhaustion and contribute to the poor acquisition of immunity in chronic infectious diseases (9). Recent studies provided evidence that the high expression of inhibitory receptors by atypical MBCs may serve to block BCR responses to soluble antigen. Kardava *et al.* (19) provided evidence

Copyright © 2020
The Authors, some
rights reserved;
exclusive licensee
American Association
for the Advancement
of Science. No claim to
original U.S. Government
Works. Distributed
under a Creative
Commons Attribution
NonCommercial
License 4.0 (CC BY-NC).

Laboratory of Immunogenetics, National Institute of Allergy and Infectious Diseases, National Institutes of Health, Rockville, MD, USA.

*Corresponding author. Email: spierce@nih.gov

that in atypical MBCs from HIV-high viremic individuals, silencing nine inhibitory receptors restored BCR cross-linking–induced proliferation. The strongest effects were observed for knockdowns of FcRL4 and Siglec-6. Conversely, we demonstrated that the expression of FcRL4 in human B cell lines blocked soluble antigen–induced BCR signaling by an FcRL4–BCR coligation-independent mechanism. Because no known ligands for these inhibitory receptors were provided in either study, it was suggested that inhibitory receptors may regulate BCR activation through their own constitutive or tonic signaling.

To our knowledge the hyporesponsiveness of BCRs expressed by atypical MBCs has been described exclusively in response to soluble antigens, generally anti-Ig as a surrogate antigen. However, current evidence indicates that in secondary lymphoid tissues *in vivo*, many antigens encountered by B cells are in immune complexes or complement fixed and associated with the surfaces of follicular dendritic cells (FDCs) through Fc receptors (FcRs) or complement receptors, the exception being low–molecular weight fully soluble antigens that appear to have free access to B cell follicles (20, 21). It is also well established that membrane-associated antigens are highly effective in triggering B cell activation (22), and several studies provided evidence that the requirements for B cell responses to soluble versus membrane-associated antigens differ in a variety of parameters including the requirement for co-receptors, response to monovalent antigens, the regulation of the cytoskeleton, and the kinetics and regulation of BCR clustering (23). For example, although B cells in CD19-deficient mice are unable to mount a proper antibody response to T cell–dependent antigens *in vivo*, B cells that lack CD19 are fully capable of responding to soluble antigens in solution *in vitro*. A possible explanation for the differences in the responses of CD19-deficient B cells *in vivo* and *in vitro* was provided by the observation that CD19-deficient B cells were defective in initiating BCR-dependent signaling in response to membrane-associated antigens *in vitro* (24). CD19-expressing B cells were shown to form active antigen–BCR–Syk microclusters that favored the transient partitioning of CD19 into the microclusters where CD19 served to amplify BCR signaling. Conversely, the inhibitory receptor CD45 appeared to be excluded from BCR–antigen microclusters. We also documented dynamic interactions of FcγRIIB with antigen–BCR microclusters independently of coligation of the BCR and FcγRIIB in B cells activated by membrane-associated antigen (25). Collectively, these studies suggest that the spatial and temporal dynamic interactions of antigen–BCR microclusters with both enhancing and inhibitory receptors may occur distinctively in response to membrane-associated antigen and not inside BCR caps generated by soluble antigen stimulation (24).

Here, we show that human atypical MBCs isolated from individuals living in malaria-endemic Africa that we previously demonstrated to be refractory to soluble antigen–induced BCR activation are fully responsive to membrane-associated antigen. Moreover, responses to membrane-bound antigen were associated with exclusion of FcγRIIB from the BCR synapse and inclusion of CD19. These results provide evidence that atypical MBCs are not exhausted and have the ability to respond to antigen *in vivo* during chronic malaria. We speculate that chronic infectious diseases promote the expansion of B cell that respond to antigens associated with cell surfaces, such as antigens in immune complexes or complement-fixed antigen, indicating that these are foreign antigens to avoid autoimmune responses to fully soluble antigens.

RESULTS

Atypical MBCs respond robustly to membrane-associated anti- λ/κ

We and others demonstrated earlier that the response of atypical MBCs to soluble anti-Ig as a surrogate antigen was highly attenuated as compared to naïve B cells and classical MBCs (10) in individuals with chronic infections. To better understand the function of atypical MBCs *in vivo*, in which case B cells are likely to encounter membrane-associated antigen on FDCs, we compared the response of atypical MBCs, naïve B cells, and classical MBCs to membrane-associated anti-Ig *in vitro*. On the basis of expression of CD19, CD21, and CD27, B cells were sorted from peripheral blood mononuclear cells (PBMCs) isolated from adults living in malaria-endemic Mali into three subpopulations: naïve B cells (CD19⁺ CD21⁺ CD27[−]), classical MBCs (CD19⁺ CD21⁺ CD27⁺), and atypical MBCs (CD19⁺ CD21[−] CD27[−]) (fig. S1A). We quantified the amount of BCR on the three subpopulations using λ/κ -specific antibodies (anti- λ/κ) and determined that naïve and classical MBCs expressed a similar amount of BCR and that atypical MBCs expressed approximately half that amount (fig. S1B). To image both unswitched (IgM) and switched (IgG) BCRs, B cells were labeled with DyLight 594–conjugated Fab IgM- or IgG-specific antibodies. B cells were placed on planar lipid bilayers (PLBs) containing F(ab')₂ anti- λ/κ as a surrogate antigen to mimic presentation of antigen to B cells by FDCs (26). As controls, B cells were placed on PLBs alone that did not contain anti- λ/κ . Cells were fixed, permeabilized, and stained with fluorescently labeled antibodies specific for the phosphorylated forms of Syk (pSyk), BLNK (pBLNK), and phospholipase C- γ 2 (PLC- γ 2) (pPLC- γ 2) and imaged by total internal reflection fluorescence (TIRF) microscopy. When placed on anti- λ/κ -containing PLBs, all IgM⁺ B cell subsets, namely, naïve B cells, classical MBCs, and atypical MBCs as well as IgG⁺ atypical and classical MBCs, accumulated BCR, pSyk, pBLNK, and pPLC- γ 2 in the immunological synapse (Fig. 1A). Quantification of BCR, pSyk, pBLNK, and pPLC- γ 2 in the images is given (Fig. 1, B and C) as is colocalization of the BCR with pSyk, pBLNK, and pPLC- γ 2 (Fig. 2). In all cases, the accumulation of BCRs (Fig. 1B) and pSyk, pBLNK, and pPLC- γ 2 (Fig. 1C) in the immune synapse were significantly higher for cells placed on anti- λ/κ -PLBs as compared to PLBs alone ($P < 0.0001$), indicating that the responses observed were dependent on BCR engagement. IgM⁺ atypical MBCs accumulated more IgM⁺ BCR at the interface of the cell and the PLBs as compared to IgM⁺ naïve B cells and IgM⁺ classical MBCs (Fig. 1B) that could reflect either a stronger response or a more rapid response by atypical MBCs given that imaging was carried out at a single time point. For IgG⁺ B cells, accumulation of IgG⁺ BCRs was similar for atypical and classical MBCs (Fig. 1B). The accumulation of both pSyk and pBLNK were similar for IgM⁺ atypical MBCs, classical MBCs, and naïve B cells but were higher compared to IgG⁺ atypical MBCs and classical MBCs. The degree of colocalization of pSyk and pBLNK with BCRs was, in all cases, greater for cells placed on anti- λ/κ -PLBs compared to PLBs alone (Fig. 2) and was similar for IgM⁺ cells of each subtype, and these were higher than the colocalization for IgG⁺ B cells. Thus, for these early kinases, accumulation of the phosphorylated forms in the synapse and colocalization with the BCRs were similar in IgM-expressing cells and greater than that of IgG-expressing cells. For the downstream kinase PLC- γ 2, the accumulation pattern was somewhat different and greatest for IgG⁺ atypical MBCs but otherwise similar for B cells of all other subpopulations (Fig. 2). In addition, IgG⁺ B cell subsets showed a

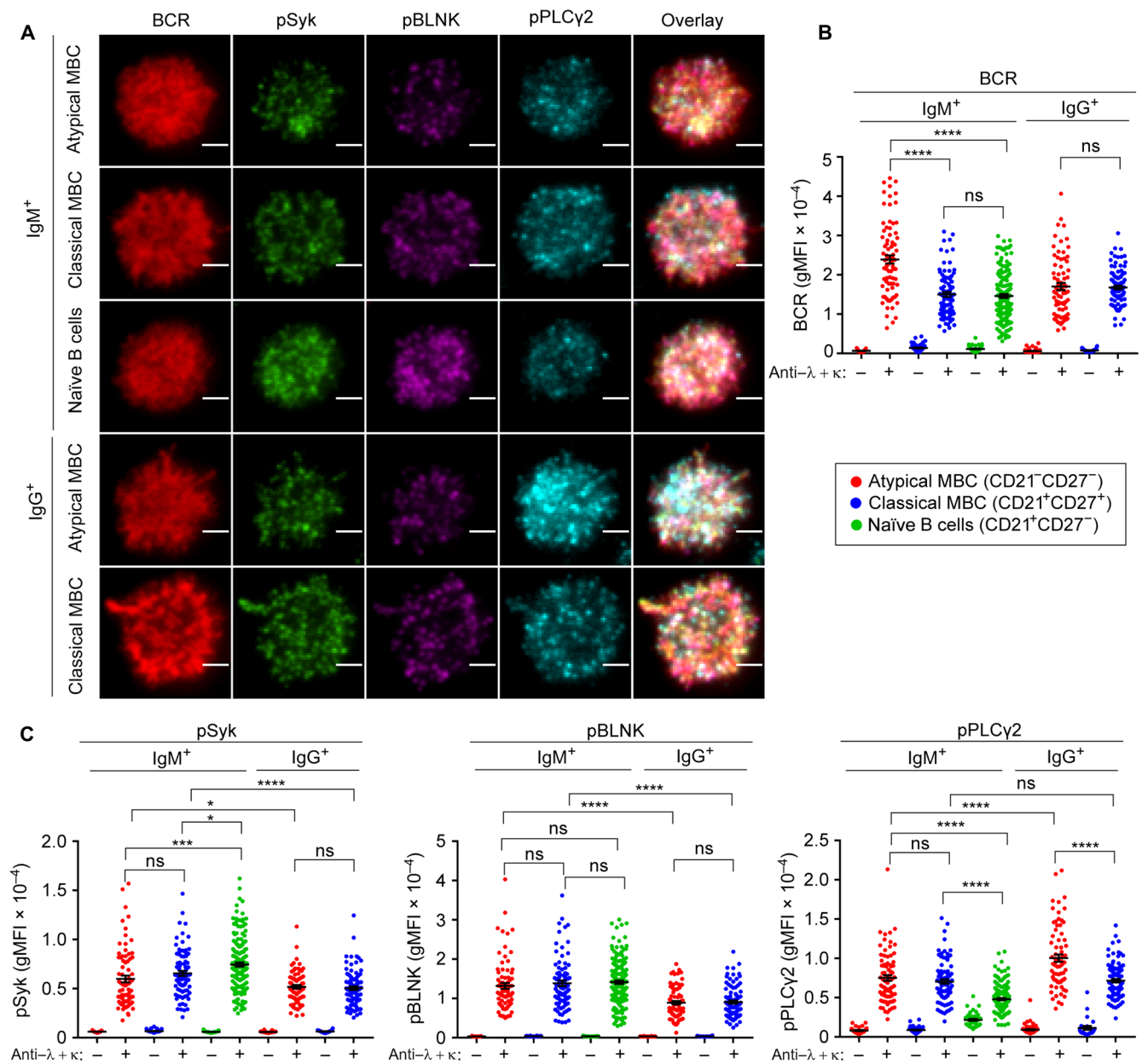


Fig. 1. Atypical MBCs signal robustly through their BCR in response to PLB-associated anti-λ/κ. Atypical MBCs (CD19⁺ CD21⁻ CD27⁻), classical MBCs (CD19⁺ CD21⁺ CD27⁺), and naïve B cells (CD19⁺ CD21⁺ CD27⁻) were fluorescence-activated cell sorting (FACS)-sorted from PBMCs, stained with DyLight 594-conjugated Fab fragments of either anti-IgM or anti-IgG, and placed on either PLBs alone or on PLBs containing anti-λ/κ for 10 min, fixed and stained with antibodies specific for the BCR and pSyk and for pBLNK and pPLC-γ2, and imaged by TIRF microscopy (see also fig. S1). (A) Representative TIRF microscopy images indicating accumulation of the BCR (IgM or IgG) (red), pSyk (green), pBLNK (magenta), and pPLC-γ2 (cyan) in the immune synapses formed by atypical MBCs, classical MBCs, and naïve B cells activated on PLBs containing anti-λ/κ (scale bar, 2 μm). (B and C) Quantification of mean fluorescence intensity (MFI) of BCR (B) and pSyk, pBLNK, and pPLC-γ2 (C) accumulated in the immune synapse of atypical MBCs (red dots), classical MBCs (blue dots), and naïve B cells (green dots) incubated on either PLBs alone or on PLBs containing anti-λ/κ. Data are representative of three experiments. The error bars indicate SEM data were analyzed using unpaired t test. **P* < 0.05; ****P* < 0.001; *****P* < 0.0001; ns, not significant.

decreased colocalization of the BCR with pPLC-γ2 following anti-λ/κ stimulation. Together, these results demonstrate that atypical MBCs are responsive to antigen if that antigen is presented on a membrane.

Atypical MBCs capture and internalize membrane-associated anti-λ/κ

Engagement of BCRs with antigen triggers internalization of the BCR-bound antigen and intracellular trafficking of the antigen

through early and late endosomes to the MHC class II compartment (MIIC) compartment where the antigen is processed and presented on MHCII. We tested the ability of atypical MBCs to internalize membrane-associated anti-λ/κ and transport the internalized anti-λ/κ to acidic endosomal compartment (Fig. 3). To do so, we used anti-λ/κ bound to flexible plasma membrane sheets (PMSs) as it was shown earlier that B cells internalize anti-λ/κ bound to the relatively inflexible PLBs only poorly (27). We used anti-λ/κ that was conjugated to a

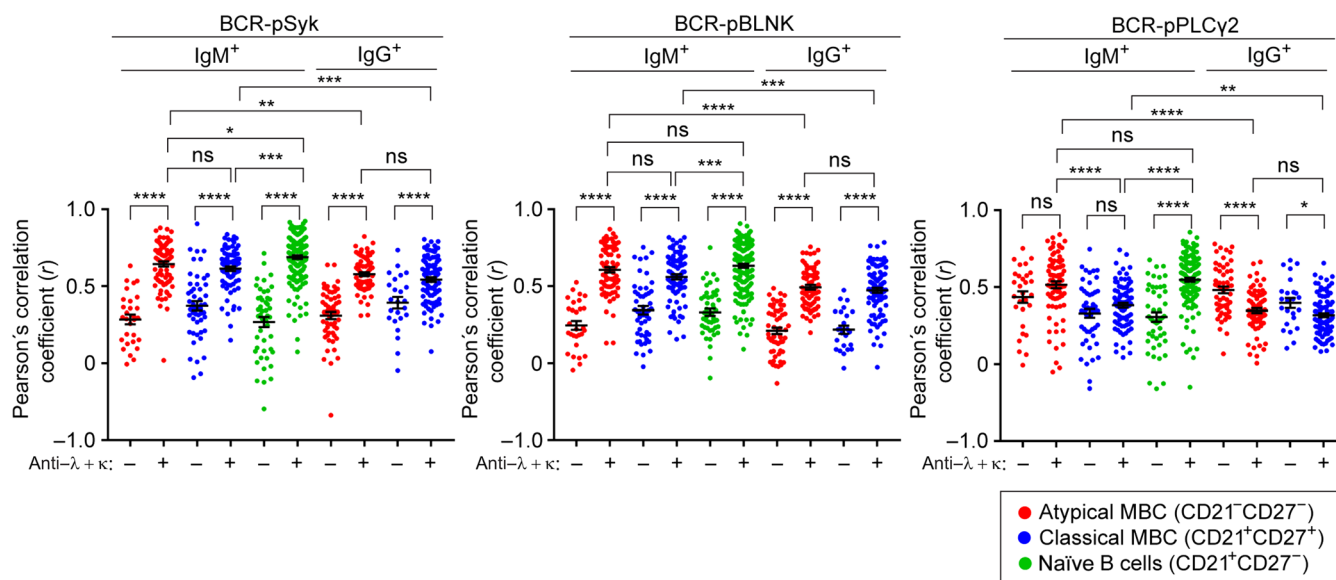


Fig. 2. Synaptic colocalization of BCR and phosphorylated signaling molecules in atypical MBCs is enhanced in response to PLB-associated anti- λ/κ . Atypical MBCs ($CD19^+ CD21^- CD27^-$), classical MBCs ($CD19^+ CD21^+ CD27^+$), and naïve B cells ($CD19^+ CD21^+ CD27^-$) were FACS-sorted from PBMCs, stained with DyLight 594-conjugated Fab fragments of either anti-IgM or anti-IgG, and placed on either PLBs alone or on PLBs containing anti- λ/κ for 10 min, fixed and stained with antibodies specific for the BCR and pSyk and for pBLNK and pPLC- $\gamma 2$ and imaged by TIRF microscopy (as in Fig. 1). Colocalization of BCR with pSyk, pBLNK, or pPLC- $\gamma 2$ within the immune synapse formed by atypical MBCs (red dots), classical MBCs (blue dots), and naïve B cells (green dots) following incubation on either PLBs alone or on PLBs containing anti- λ/κ . Data are representative of three experiments. The error bars indicate SEM. Data were analyzed using unpaired *t* test. * $P < 0.05$; ** $P < 0.01$; *** $P < 0.001$; **** $P < 0.0001$; ns, not significant.

pH-insensitive fluorescence dye, DyLight 650, and biotinylated and bound to PMS followed by binding of an avidin-conjugated pH-sensitive dye, pHrodo, to anti- λ/κ . Purified B cells were placed on PMS-DyLight 650-pHrodo-anti- λ/κ for increased periods of time up to 120 min. At each time point, the cells were harvested from the PMS and stained with antibodies specific for CD19, CD21, and CD27 and analyzed by flow cytometry to determine the amount of anti- λ/κ captured and internalized by naïve B cells ($CD19^+ CD21^+ CD27^-$), classical MBCs ($CD19^+ CD21^+ CD27^+$), and atypical MBCs ($CD19^+ CD21^- CD27^-$) (fig. S2). The amount of captured anti- λ/κ that remained on the B cell surface at each time point was determined by staining cells with streptavidin-Alexa Fluor 488 that bound to biotinylated anti- λ/κ on the surface. The fraction of the captured anti- λ/κ that was internalized was determined by comparing the amount of anti- λ/κ on the surface [Alexa Fluor 488 FI (fluorescence intensity)] to the total amount of anti- λ/κ acquired by the B cells (DyLight 650 FI). Atypical MBCs captured more anti- λ/κ as compared to classical MBCs and naïve B cells after incubation on anti- λ/κ -containing PMS for 30 to 120 min (Fig. 3A). Similarly, the amount of anti- λ/κ internalized was higher in atypical MBCs as compared to classical MBCs or naïve B cells (Fig. 3B). The ability of atypical MBCs to capture and internalize more anti- λ/κ may be attributable, at least in part, to the observation that atypical MBCs spread over a larger area on the anti- λ/κ -containing PMS as compared to classical MBCs and naïve B cells (fig. S1D) despite the fact that they express less BCR (fig. S1B).

Both the percent of B cells that took up anti- λ/κ as measured by pHrodo FI (Fig. 3C, left) and the FI of pHrodo per cell (Fig. 3C, middle) increased from 30 to 120 min for atypical MBCs, classical MBCs, and naïve B cells, indicating that B cells of all subpopulations trafficked internalized anti- λ/κ to increasingly acidic compartments over 120 min (Fig. 3C). Atypical MBCs appeared to traffic larger

amounts of anti- λ/κ to the acidic compartments as compared to classical MBCs or naïve B cells (Fig. 3C). However, since atypical MBCs captured and internalized more anti- λ/κ than classical MBCs or naïve B cells, when the pHrodo FI was normalized to the FI of captured anti- λ/κ , all cells trafficked a similar proportion of the anti- λ/κ that they acquired (Fig. 3C, right). Together, these data provide evidence that the capture and internalization and trafficking of anti- λ/κ by atypical MBCs was at least comparable to, if not greater than, that of classical MBCs and naïve B cells.

The spatial distribution of internalized anti- λ/κ and microtubule-organizing center polarization distinguish atypical MBCs

We characterized the spatial distribution of anti- λ/κ captured and internalized by the B cell subpopulations. Sorted B cell subpopulations were placed on PMS-containing DyLight 550-labeled anti- λ/κ for 30 to 90 min, fixed and permeabilized and stained with fluorescently labeled antibodies specific for human leukocyte antigen-DR (HLA-DR). Shown are the confocal images through the *Z* section (Fig. 4A). After 30 min, HLA-DR appeared to be evenly distributed on the cell surface for each subset. B cells of each subset accumulated internalized anti- λ/κ at the contact site of the B cells with the PMS confirmed by quantifying the distance of the anti- λ/κ from the PMS (Fig. 4, A and B). Unexpectedly, after 90 min of incubation, atypical MBCs had trafficked the anti- λ/κ away from the contact site to the opposite pole of the cell (Fig. 4A), in contrast to classical MBCs and naïve B cells in which the anti- λ/κ remained proximal to the contact site (Fig. 4A). The distance of the internalized anti- λ/κ from the PMS was quantified for each cell population and showed that for naïve B cells and classical MBCs, anti- λ/κ was concentrated in close proximity to the membrane, but in atypical

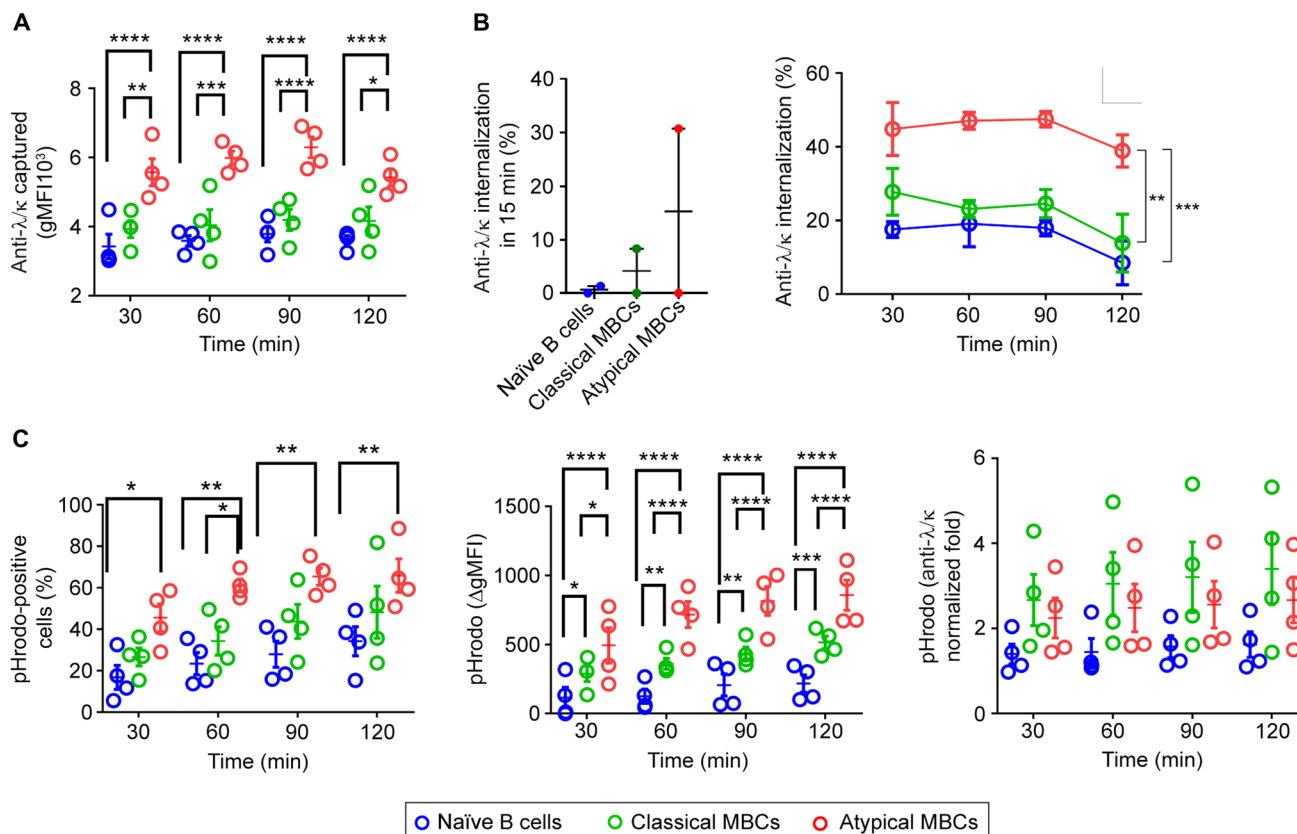


Fig. 3. Atypical MBCs rapidly capture and internalize PMS-bound anti- λ/κ . PBMCs were incubated for increasing lengths of time (30 to 120 min) at 37°C on PMS containing biotinylated anti- λ/κ conjugated to DyLight 650 and avidin-pHrodo. At each time point, cells were harvested and stained with streptavidin-Alexa488 and antibodies specific for CD19, CD21, and CD27 to identify naïve B cells (CD19⁺ CD21⁺ CD27⁻), classical MBCs (CD19⁺ CD21⁺ CD27⁺), and atypical MBCs (CD19⁺ CD21⁻ CD27⁻). Antigen capture, internalization, and trafficking into the acidic compartments were analyzed by flow cytometry as described in the text and detailed in Materials and Methods ($n = 4$). In all cases: atypical MBCs (red circles), classical MBCs (green circles), and naïve B cells (blue circles) (see also fig. S2). **(A)** Comparison of the total amount of anti- λ/κ captured from PMS over time indicated by the MFI of DyLight 650. **(B)** Comparison of the amount of anti- λ/κ internalized in 15 min (left) and over time (right). **(C)** Comparison of anti- λ/κ trafficking to acidic compartment over time indicated by the percentage of cells positive for pHrodo or by the increases in pHrodo MFI from time 0. Data were analyzed using paired t test (A and C) or two-way analysis of variance (ANOVA) and Tukey's multiple comparison test (B). * $P < 0.05$; ** $P < 0.01$; *** $P < 0.001$; **** $P < 0.0001$.

MBCs, the anti- λ/κ spread across the cell to the opposite pole (Fig. 4B).

This same pattern of anti- λ/κ polarization in atypical MBCs as compared to naïve B cells and classical MBCs is apparent in confocal sections of the cells labeled with antibodies specific for HLA-DR and LAMP-1, a marker for late endosomes and the MIIC (Fig. 4C). Confocal images indicate that LAMP-1⁺ vesicles accumulated proximal to the PMS for naïve B cells and classical MBCs but are distributed at distances away from the PMS in atypical MBCs, a distribution similar to that observed for anti- λ/κ (Fig. 4C). The recruitment of anti- λ/κ into the vesicles containing HLA-DR and LAMP-1, as indicated by three-dimensional (3D) colocalization of anti- λ/κ , HLA-DR, and LAMP-1, is similar for atypical MBCs, classical MBCs, and naïve B cells (Fig. 4D).

It was earlier shown that in B cells activated on membrane-associated antigen, the microtubule-organizing centers (MTOCs) polarized toward the interface of B cells with antigen-containing membranes (28). Consistent with this observation, in naïve B cells and classical MBCs, the MTOCs stained with antibodies specific for γ -tubulin appeared polarized proximal to anti- λ/κ -containing PMS at 90 min

(Fig. 4E). In contrast, the MTOCs in atypical MBCs were not polarized toward the immune synapse at this time point (Fig. 4E). The degree of polarization of MTOCs was quantified for a large number of cells by calculating the polarity index of MTOCs, which was significantly higher for atypical MBCs with the index >0.5 in average as compared to classical MBCs and naïve B cells with the index <0.5 (Fig. 4F). Thus, the atypical MBCs internalize the anti- λ/κ and trafficked it to sites distal from the immune synapse, which is accompanied by loss of MTOC polarity toward the PMS.

Membrane-associated anti- λ/κ induced the expression of the early PC differentiation marker IRF4 in atypical MBCs

IRF4 is an essential transcription factor for differentiation of B cells to PCs (29). The balance of the expression of the transcription factors IRF4 and IRF8 determines a PC versus germinal center (GC) B cell fate, with a high IRF4-to-IRF8 ratio promoting PC differentiation (30). We quantified IRF4 and IRF8 mRNA levels in sorted naïve B cells, classical MBCs, and atypical MBCs in response to soluble versus membrane-associated anti- λ/κ after 24-hour incubation in the presence of the TLR9 agonist CpG and BAFF and the cytokines

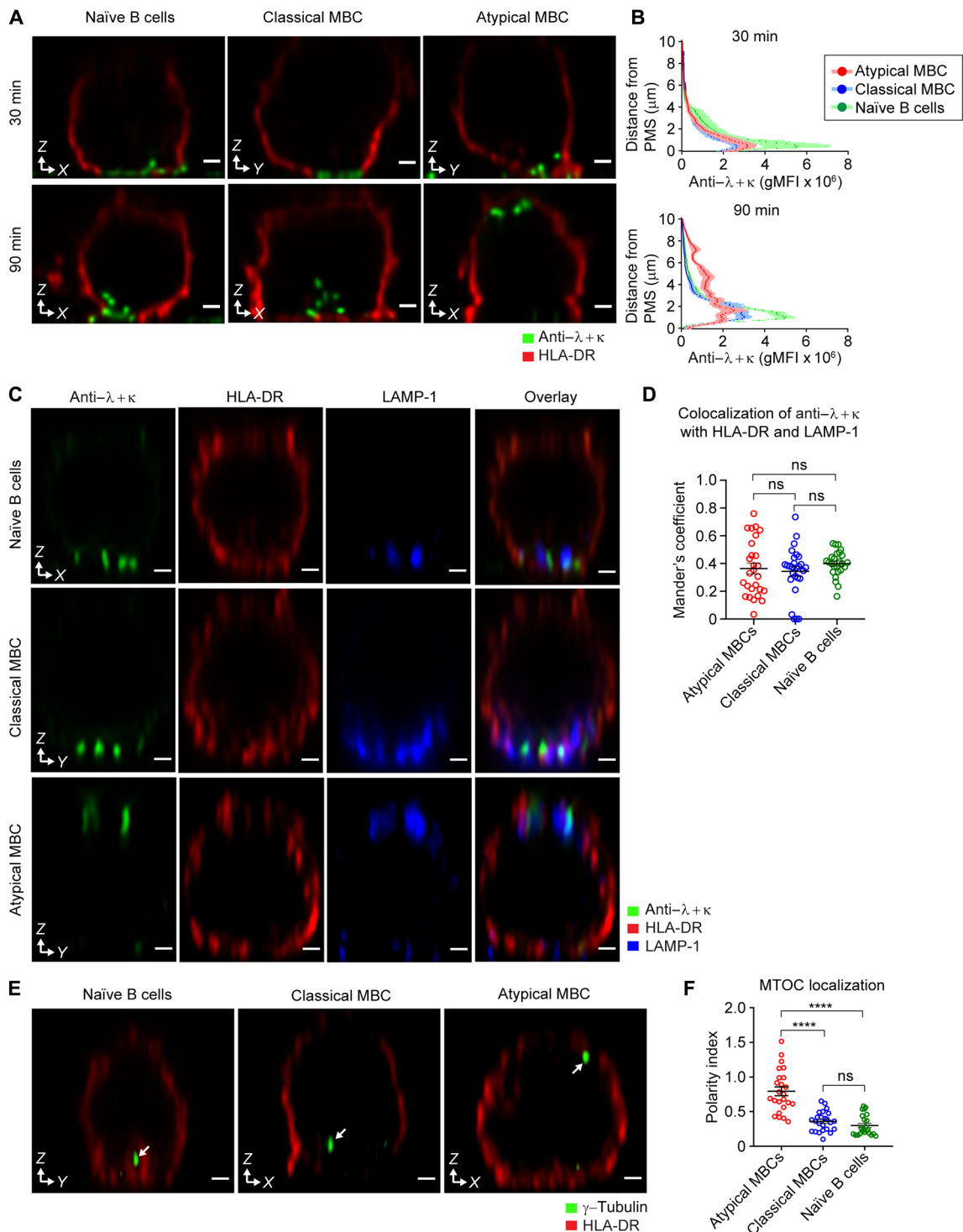


Fig. 4. Atypical MBCs show a distinct orientation when gathering, internalizing, and trafficking anti- λ/κ from PMS. Atypical MBC, classical MBCs, and naïve B cells were FACS-sorted from PBMCs and activated for 30 or 90 min at 37°C on PMS containing anti- λ/κ conjugated to DyLight 550 and fixed and stained with various antibodies imaged by confocal microscope. **(A)** Representative images showing anti- λ/κ (green) and HLA-DR (red) in orthogonal confocal sections of cells incubated on PMS containing anti- λ/κ for 30 and 90 min (scale bar, 1 μ m). **(B)** Quantification of the distance of the anti- λ/κ from the PMS after 30 and 90 min of incubation of anti- λ/κ -containing PMS. **(C)** Representative images showing anti- λ/κ (green), HLA-DR (red), and LAMP-1 (blue) in orthogonal confocal sections of cells incubated on PMS containing anti- λ/κ for 90 min (scale bar, 1 μ m). **(D)** 3D colocalization of anti- λ/κ with HLA-DR and LAMP-1 (Mander's coefficient) in each B cell subpopulation. **(E)** Representative images indicating γ -tubulin (green) and HLA-DR (red) in orthogonal confocal sections of cells incubated on PMS containing anti- λ/κ for 90 min. The arrows indicate the location of MTOCs in the cell (scale bar, 1 μ m). **(F)** Polarity index for the localization of MTOCs in each B cell subpopulation. Data are representative of two experiments. The error bars indicate SEM. Data were analyzed using a one-way ANOVA and Tukey's multiple comparison test. **** $P < 0.0001$; ns, not significant.

IL-21, IL-2, and IL-10, conditions reported to induce differentiation to PC (15). Relative levels of expression of IRF4 and IRF8 mRNA were determined by quantitative real-time polymerase chain reaction (qRT-PCR) and quantified by the $2^{-\Delta\Delta Ct}$ method. Data are expressed as the fold change in expression by stimulated cells compared to cells cultured in vitro for 24 hours in media alone. For atypical MBCs, the relative levels of IRF4 expression were significantly higher in response to PLB-associated anti- λ/κ as compared to soluble anti- λ/κ (Fig. 5A), whereas the levels of IRF8 were similar for both (Fig. 5B), resulting in a significantly higher ratio of IRF4-to-IRF8 expression (Fig. 5C). In contrast, for both classical MBCs and naïve B cells, the expression of both IRF4 and IRF8 was not significantly different in response to soluble anti- λ/κ and PLB-associated anti- λ/κ (Fig. 5, A and B), resulting in IRF4-to-IRF8 expression ratios that were not significantly different (Fig. 5C). These results show that the differential ability of atypical MBCs to respond to soluble versus membrane-associated anti- λ/κ correlates with the fate of the B cells to PC differentiation.

Atypical MBCs exclude the inhibitory co-receptor Fc γ RIIB from the immune synapse in response to membrane-associated anti- λ/κ

Because a characteristic feature of atypical MBCs is their high expression of inhibitory receptors including Fc γ RIIB, we sought to determine whether the ability of atypical MBCs to respond to membrane-associated antigen was due to alterations in the temporal or spatial distribution of the BCR and the inhibitory receptor Fc γ RIIB or the enhancing co-receptor CD19 during activation. Sorted B cell subpopulations were stained with Alexa Fluor 488-conjugated F(ab) CD19-specific antibodies and DyLight 594-conjugated F(ab) IgM- or IgG-specific antibodies, and the cells were placed on PLBs containing anti- λ/κ for increased periods of time (1, 2, and 10 min). At the end of each time point, cells were fixed on the PLBs and stained with primary antibodies specific for Fc γ RIIB, followed by Alexa Fluor 647-labeled Ig-specific secondary antibodies and imaged by TIRF microscopy. The B cells of each subpopulation spread over the bilayer and accumulated BCR, Fc γ RIIB, and CD19 at the interface

(Fig. 6). We quantified the total amount of BCR, Fc γ RIIB, and CD19 that accumulated at the interface of the B cell and the bilayer with time and observed that, as expected, the amount of BCR increased for all B cell subpopulations over 10 min (fig. S3A). However, the total amount of Fc γ RIIB and of CD19 decreased over the 10-min time course for all B cell subpopulations with the exception of naïve B cells that showed only a transient decrease in Fc γ RIIB and CD19 at 2 min. We do not know whether the decreases were a result of internalization, recycling, or movement out of the contact site and whether the cause of the decrease was similar for Fc γ RIIB and CD19. We quantified the spatial distribution of the BCR, Fc γ RIIB, and CD19 across the interface for the B cells shown in Fig. 6. The mean fluorescence intensity (MFI) was recorded across the midline of each cell as indicated by the white lines (Fig. 6). At 1 min, for all cell populations, BCR, Fc γ RIIB, and CD19 were distributed similarly across the cell. However, at 2 min, the distribution of Fc γ RIIB began to be skewed toward the periphery, and by 10 min, there was a clear accumulation of the Fc γ RIIB toward the cell's periphery. In contrast, the distribution of the BCR and CD19 did not change noticeably.

We quantified the distribution for a large number of cells by defining a region of interest (ROI) that encompassed the center of the cell with the highest BCR accumulation (Fig. 7A). We then measured the MFI in the ROI in the center and outside the ROI in the periphery and expressed these values as a ratio of Geometric mean fluorescence intensity (gMFI) center: gMFI periphery. A ratio of 1 indicates equal distribution in the center and periphery; a ratio >1 indicates greater accumulation in the cell center as compared to the periphery, and a ratio <1 indicates greater accumulation in the periphery as compared to the center (Fig. 7A). As clearly shown, with time as the BCR accumulated in the cell center, Fc γ RIIB was excluded from the center and accumulated in the periphery (Fig. 7, B and C). In contrast, CD19 remained relatively evenly distributed across the IgG⁺ cells and showed a modest increase in the center for IgM⁺ cells (Fig. 7D). Thus, as the BCR synapse formed in the center of the cell where the BCR accumulated, Fc γ RIIB was excluded and CD19 was included.

We also determined the pairwise colocalization of the BCR and Fc γ RIIB and the BCR and CD19 for a large number of cells,

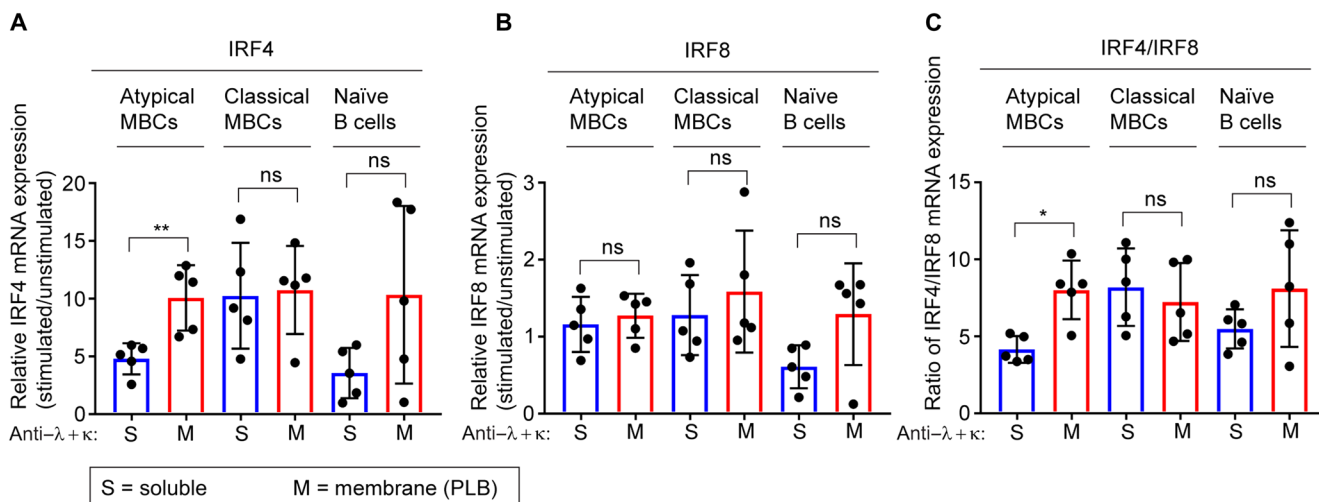


Fig. 5. Atypical MBCs express IRF4 upon responding to PLB-associated anti- λ/κ . Relative mRNA expression level of IRF4 (A), IRF8 (B), and ratio of IRF4/IRF8 (C) in FACS-sorted atypical MBC, classical MBCs, and naïve B cells after in vitro activation with PLB-bound anti- λ/κ or soluble anti- λ/κ , along with TLR9 agonist CpG, BAFF, and cytokines IL-2, IL-10, and IL-21 ($n = 5$). The error bars indicate SD. Data were analyzed using nonparametric Mann-Whitney test. * $P < 0.05$; ** $P < 0.01$; ns, not significant.

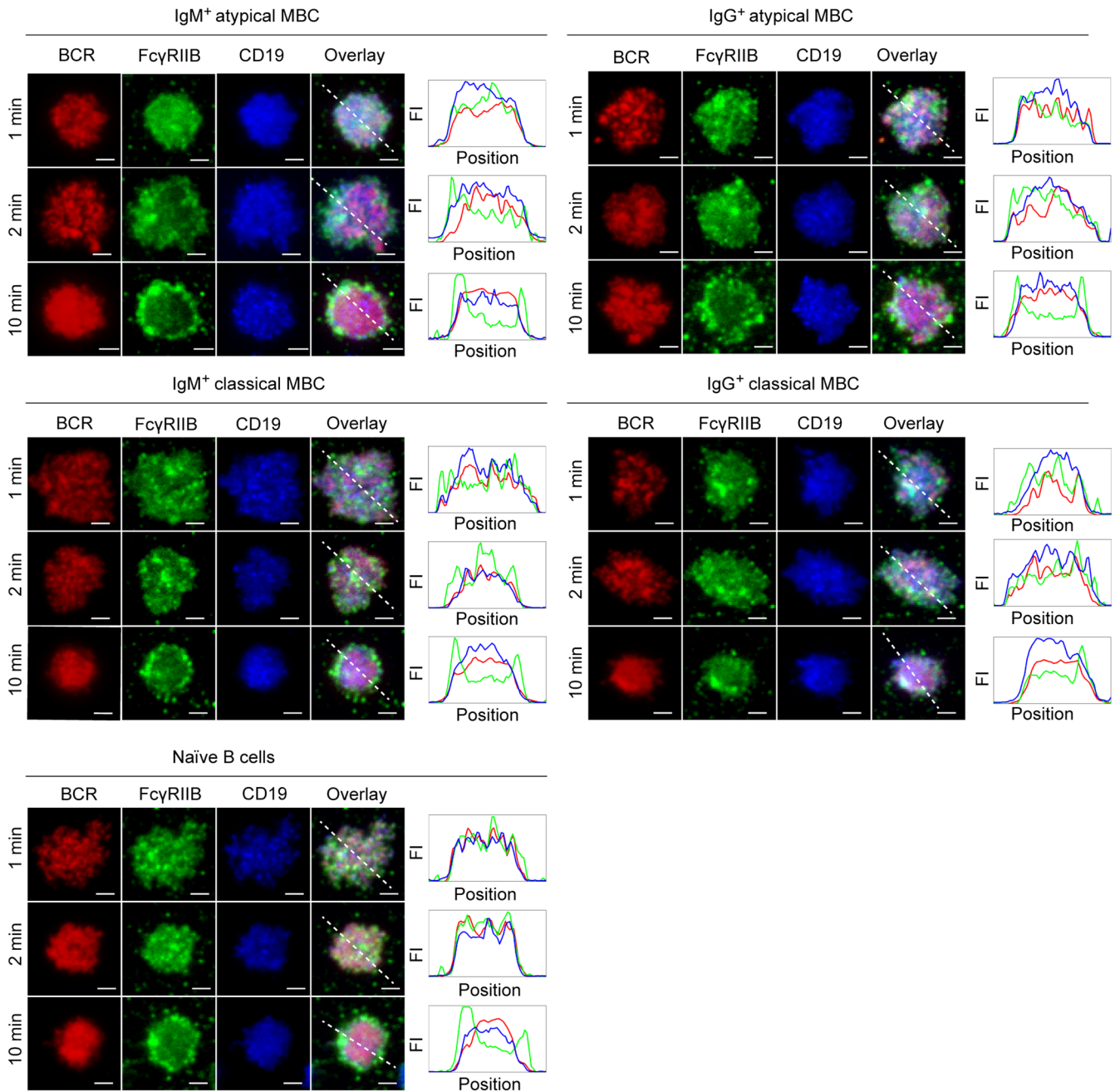


Fig. 6. Atypical MBCs rapidly segregate Fc γ RIIB to periphery of immune synapse formed on PLB-associated anti- λ/κ . Atypical MBCs, classical MBCs, and naïve B cells were FACS-sorted from PBMCs, stained with DyLight 594-conjugated Fab fragments of either anti-IgM or anti-IgG and Alexa Fluor 488-conjugated Fab fragments of anti-CD19 antibodies, and activated on PLBs containing anti- λ/κ for 1 to 10 min, fixed and stained with antibodies recognizing Fc γ RIIB, and imaged by TIRF microscopy. Representative TIRF microscopy images indicating localization of the BCR (IgM or IgG) (red), Fc γ RIIB (green), and CD19 (blue) within immune synapses formed by atypical MBCs, classical MBCs, and naïve B cells activated on PLBs containing anti- λ/κ . Relative FI along the dashed white line is given (scale bar, 2 μ m).

calculated as a Pearson's correlation coefficient. Colocalization provides a finer description of the distribution of the receptors at a molecular level as compared to the analysis of the center/periphery distribution. As predicted by the exclusion of the Fc γ RIIB from the center of the cell with time, the colocalization of the BCR and Fc γ RIIB decreased with time, most markedly for the atypical MBCs showing more negative correlation by 10 min, especially in IgM⁺ cells (fig. S3B). However, the picture for CD19 was more complicated

and appeared to correlate with the isotype of the BCR. For IgM⁺ atypical MBCs, the colocalization with CD19 decreased by 10 min but remained constant for IgG⁺ atypical MBCs although the accumulation of CD19 decreased for both IgM⁺ and IgG⁺ atypical MBCs. IgM⁺ classical MBCs, in contrast, showed increased BCR/CD19 colocalization by 10 min, but colocalization for IgG⁺ classical MBCs remained constant. For naïve B cells, there was no detectable change. As the distribution of CD19 was skewed with time toward

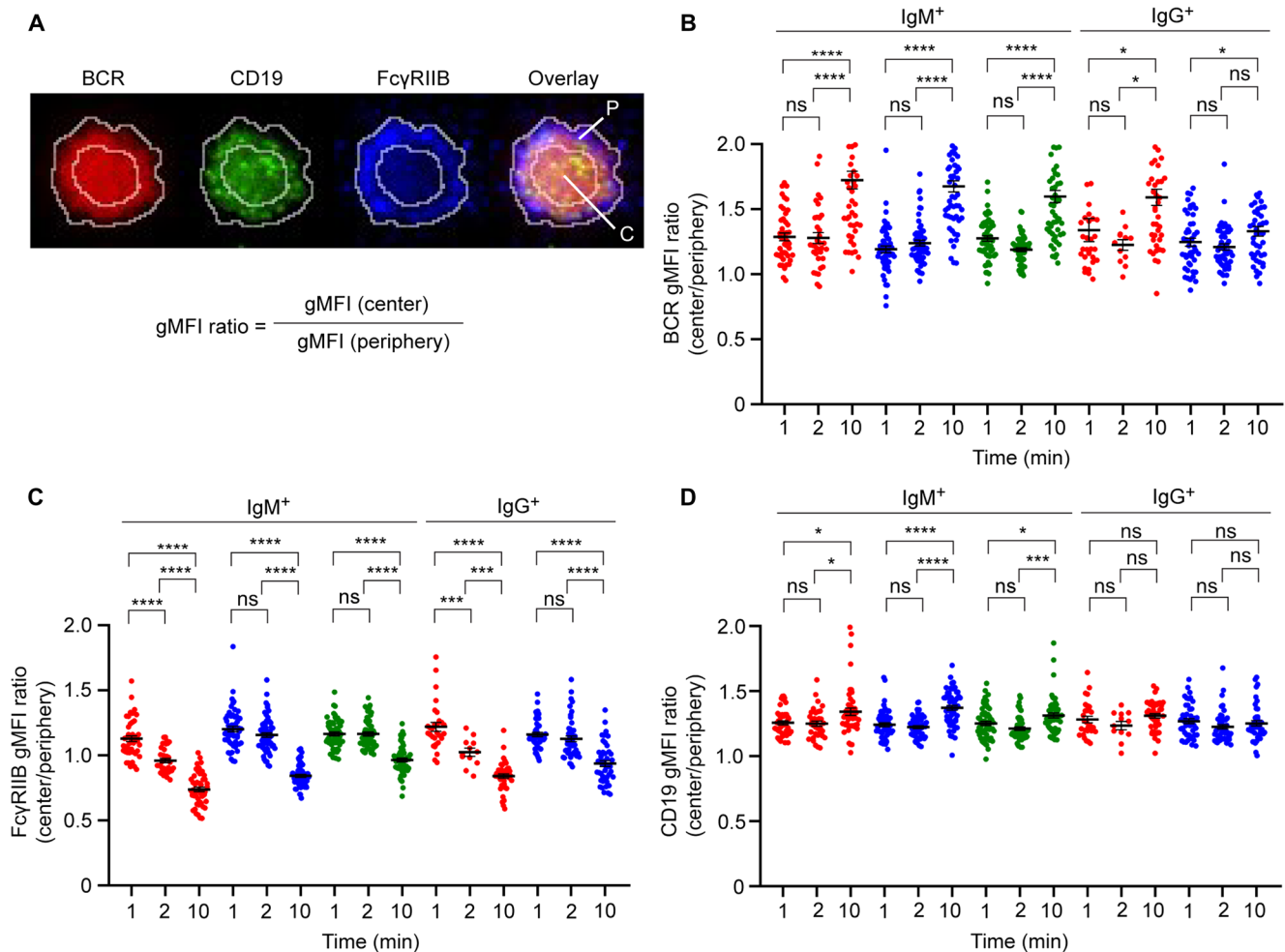


Fig. 7. Segregation of Fc γ RIIB to the cell periphery is accompanied by accumulation of BCR and CD19 in the immune synapse of atypical MBCs responding to PLB-associated anti- λ/κ . Atypical MBCs, classical MBCs, and naïve B cells were FACS-sorted from PBMCs, stained with DyLight 594–conjugated Fab fragments of either anti-IgM or anti-IgG and Alexa Fluor 488–conjugated Fab fragments of anti-CD19 antibodies, and activated on PLBs containing anti- λ/κ for 1 to 10 min, fixed and stained with antibodies recognizing Fc γ RIIB, and imaged by TIRF microscopy (as in Fig. 6) (see also fig. S3). **(A)** Representative TIRF microscopy image indicating localization of the BCR (red), CD19 (green), and Fc γ RIIB (blue) within immune synapses. White line indicates the ROI selected for calculating the MFI in the center (shown as C in overlay) and in the periphery (shown as P in overlay) of the immune synapse. **(B to D)** Quantification of ratio of MFI in center versus periphery of the immune synapse for BCR (B), Fc γ RIIB (C), and CD19 (D) in atypical MBCs (red dots), classical MBCs (blue dots), and naïve B cells (green dots) activated on PLBs containing anti- λ/κ . Data are representative of two experiments. The error bars indicate SEM. Data were analyzed using unpaired *t* test. **P* < 0.05; ****P* < 0.001; *****P* < 0.0001; ns, not significant.

the cell center, these data may suggest a more dynamic relationship of IgM BCRs with CD19 cells as compared to IgG BCRs.

Together, these findings provide evidence that B cells, when engaged with membrane-bound antigens, segregate away from Fc γ RIIB, thus minimizing inhibition of BCR signaling, and remain in contact with CD19, providing enhancement of BCR responses.

DISCUSSION

Here, we show that atypical MBCs from individuals chronically exposed to malaria are not hyporesponsive to antigen as previously assumed on the basis of their response to soluble antigen but rather fully capable of responding to antigen when presented on membranes including BCR signaling, antigen gathering, and internalization and differentiation toward the PC lineage. This selectivity in responding to membrane-associated antigen but not to soluble antigen is

unique to atypical MBC and not observed for naïve B cells or classical MBCs from the same individuals that respond similarly to soluble and membrane-associated antigens. In addition, the results presented here identified several previously unknown features of the mechanisms by which atypical MBCs engage membrane-associated antigen, extract it, and internalize it for presentation as compared to naïve B cells and classical MBCs that might provide clues as to the function of atypical MBCs.

To our knowledge, this is the first example of the restriction of B cells of a particular differentiated subset to respond to membrane-associated versus soluble antigen. Our observations raise the question: Does the restriction of atypical MBCs to membrane-associated antigen observed here *in vitro* play a role *in vivo* during chronic infectious diseases? At present, we can only speculate. B cells first encounter antigen in the B cell follicles of secondary lymphoid organs (SLOs) (20). Antigens arrive in the SLO through afferent

lymphatics via subcapsular sinuses (SCSs). Lymphoid endothelial cells together with a network of surrounding macrophages create a tight barrier that prevents movement of large antigens and antigen complexes into B cell follicles (31). The exception appears to be small antigens, estimated to be under 70 kDa, that have been shown to rapidly penetrate B cell follicles through lymphatic conduits within minutes after entering the SCSs (20, 32, 33). Larger antigens (>70 kDa), viruses, and viral-like particles in the form of immune complexes or complement-coupled complexes are captured by FcR- and complement receptor-expressing SCS macrophages. Antigen complexes are rapidly shuttled to noncognate B cells that transport the antigen complexes into follicles where the complexes are deposited onto FDCs that provide a continuous supply of antigen during the B cell response (34). Thus, during chronic infections, atypical MBCs in SLO would be potentially exposed to both soluble and membrane-associated antigens, but our data indicate that they would only respond to the membrane-associated antigens. It may be that high concentrations of soluble antigens accumulate in chronic infections and that these high levels are deleterious to atypical MBCs, resulting in cyclic initiation and inhibition of signaling cascades from which the B cell cannot recover. It is even possible that chronic soluble antigen encounters are responsible for driving the differentiation of atypical MBCs initially. However, our recently published data defining the conditions *in vitro* that drive naïve human B cells to acquire the phenotypic and functional characteristics of atypical MBCs, including hyporesponsiveness to soluble antigen, showed that antigen associated with stiff membranes from which the B cells could not internalize antigen but continually engaged it was more effective than soluble antigen in inducing atypical MBCs (35). Nonetheless, acquiring a phenotype that blinds atypical MBCs to soluble antigen may be essential to rescue the B cell's potential function by limiting responses to membrane-associated antigen.

We also observed several unusual features of the mechanisms of antigen engagement by atypical MBCs as compared to naïve and classical MBCs. The most notable was the failure of atypical MBCs to polarize toward the plane of the contact site with the antigen-containing membrane in which the synapse formed. Atypical MBCs, like naïve and classical MBCs, initially bound and accumulated BCRs at the site of contact with the antigen-containing membrane. However, unlike naïve and classical MBCs that polarized the MTOCs toward the contact site and internalized BCR-antigen complexes from the contact site, atypical MBCs did not polarize the MTOCs toward the contact site and transported BCR-antigen complexes away from the contact site. Otherwise, some of transferred BCR-antigen complexes from PMS might move along the outside of the cell for internalization into processing compartments at the opposite pole. It is possible that this unusual orientation of processed antigen plays a role in atypical MBC interactions with T cells, perhaps by not requiring the B cell to completely disengage from the antigen-presenting FDC to interact with T cells. In this regard, it is of interest that atypical MBCs showed an activated phenotype immediately *ex vivo* with higher basal levels of phosphorylated BCR signaling molecules, most notably Syk and PLC- γ 2 (18, 36). High basal phosphorylation of BCR signaling molecules was also observed for atypical MBCs in HIV infections (37) and COVID (Common Variable Immune Deficiency) (38). It might be that atypical MBCs remain associated with antigen-presenting cells *in vivo* longer, resulting in prolonged activation. It is also of interest that we observed this unusual orientation of antigen internalization in human GC B cells (39) first

described for mouse GC B cells (40). The defining feature of GC B cells described in our study was their ability to discriminate high- versus low-affinity membrane-associated antigens due to their inherent high-affinity threshold for antigen. In GC light zones, the affinity selection of B cells is ultimately dependent on the ability of GC B cells to activate and receive help from T follicular helper cells (41). It is possible that the unusual orientation of antigen internalization serves a similar purpose in both atypical MBCs and GC B cells, possibly related to interactions with T cells. The studies presented here focused on a comparison of atypical MBC, classical MBCs, and naïve B cells within individuals chronically exposed to malaria. The finding of a functional distinction between responses to antigens among these three B cell subpopulations associated with chronic infection raises the question: Does chronic malaria infection also affect functional features of naïve B cells and classical MBCs? A robust comparison of naïve and classical MBCs from Malian and U.S. donors, particularly at the single-cell level, will be necessary to address this interesting possibility.

Last, the results described here provide a potential mechanism underlying the inability of atypical MBCs to respond to soluble antigen, namely, the characteristic high expression of inhibitory receptors. On the basis of studies of the differential requirement for CD19 in B cells responding to soluble versus membrane-associated antigen, in which spatial and temporal dynamic interactions of antigen-BCR microclusters with CD19 were observed in B cells responding to membrane-associated antigen, Batista and colleagues suggested that these interactions may not occur inside BCR caps generated by soluble antigen engagement (24). We observed that the inhibitory BCR Fc γ RIIB was segregated away from BCRs in atypical MBCs in the contact area of the B cell with membrane-associated antigen, whereas the activating receptor CD19 was included in areas in which BCRs accumulated. Inclusion of CD19 would serve to amplify signals through the BCR through its recruitment of Src family kinases, while the exclusion of Fc γ RIIB would negate the impact of its recruitment of the phosphatase SHIP1 [Src homology 2 (SH2) domain containing inositol polyphosphate 5-phosphatase 1] (42, 43) on BCR microcluster signaling (44).

In addition, the Fc γ RIIB also regulates PC differentiation through its ability to control B cell activation. For example, B cells expressing DNA-specific BCRs differentiate into CD138⁺ PCs in Fc γ RIIB-deficient mice (45). In addition, coengagement of the Fc γ RIIB and the BCR inhibits the *in vitro* differentiation of human B cells to PCs (46), and the engagement of Fc γ RIIB alone affects persistence of PC in bone marrow (47). Thus, exclusion of the Fc γ RIIB from the BCR clusters would also be predicted to enhance differentiation of atypical MBC to PC as shown here. Moreover, the levels of both CD19 and Fc γ RIIB are elevated in atypical MBCs (18, 48) such that in soluble antigen stimulation, the BCRs would encounter high levels of the inhibitory receptor and in stimulation by membrane-associated antigen, high levels of the enhancing receptor CD19 in the absence of Fc γ RIIB would promote BCR signaling. In addition, the findings presented here are consistent with those of Kardava *et al.* (19) that showed that knockdown of the expression of inhibitory receptors on atypical MBCs from HIV-viremic individuals resulted in the gain of responsiveness to soluble antigen.

The observation that the exclusion of Fc γ RIIB away from the BCR clusters at the interface of the atypical MBCs and the antigen-containing PLBs was associated with BCR signaling raises the question: Do other inhibitory receptors expressed by atypical MBCs function to block BCR signaling, and if so, are these also excluded from BCR

clusters? We previously showed that the surface expression of FcRL5 is bimodal on atypical MBCs with approximately 40% of atypical MBCs expressing FcRL5 and signaling induced by BCR cross-linking of these FcRL5⁺ atypical MBCs by soluble antigen was reduced as compared to FcRL5⁻ atypical MBCs indicating that FcRL5 expression was sufficient to block BCR signaling to soluble antigens (18). If the expression of FcRL5 were also sufficient to dampen the response of atypical MBCs to membrane-associated antigen, then we would expect a bimodal response in the studies presented here. However, there was no evidence for such a bimodal response (see Figs. 1 and 5), suggesting that FcRL5 is also excluded along with FcγRIIB from BCR clusters activated by membrane-associated antigen.

At present, we do not have an understanding of the function of atypical MBCs in chronic infectious diseases. However, the results presented here showing that atypical MBCs are activated in response to membrane-associated antigen and that they appear to have the potential both to present antigen to T cells and to differentiate toward PCs will likely benefit future efforts to understand the function of this highly expanded B cell subpopulation in chronic infectious diseases and autoimmunity.

MATERIALS AND METHODS

Study participants

Malian donors' PBMCs were obtained from individuals enrolled in a cohort study [National Institute of Allergy and Infectious Diseases (NIAID) protocol 07-I-N141 or 06-I-N147] approved by the ethics committee of the Faculty of Medicine, Pharmacy, and Dentistry at the University of Sciences, Techniques, and Technologies of Bamako, in Mali and reviewed by the National Institutes of Health (NIH) Institutional Review Board. Informed consent was obtained from all participants. This study was conducted in the rural village of Kalifabougou, Mali where intense *Plasmodium falciparum* transmission occurs from June through December each year.

Fluorescence-activated cell sorting of B cells

B cell subpopulations from PBMCs were sorted on the basis of expression of CD19, CD21, and CD27 into naïve B cells (CD19⁺ CD21⁺ CD27⁻), classical MBCs (CD19⁺ CD21⁺ CD27⁺), and atypical MBCs (CD19⁺ CD21⁻ CD27⁻) using a FACSAria II or FACSAria Fusion cell sorter (BD Biosciences) (fig. S1A).

Preparation of artificial antigen-presenting membranes

PLBs were prepared as previously described (49) in individual chambers formed by securing a CultureWell reusable silicone gasket (Grace Bio-Labs) to 24 mm by 50 mm, #1.5 Borosilicate cover glass. Briefly, PLBs were prepared using 110 μM small unilamellar vesicles consisting of 1,2-dioleoyl-*sn*-glycerol-3-phosphocholine (DOPC) and 1,2-dioleoyl-*sn*-glycerol-3-phosphoethanolamine-*N*-(cap biotinyl) (DOPE-cap biotin) (Avanti Polar Lipids) in ratio 100:1. To bind anti-λ/κ to the PLBs, the wells containing PLBs were incubated at room temperature (RT) with streptavidin (2.5 μg/ml) for 10 min, followed by biotinylated goat F(ab')₂ anti-human λ + κ (1 μg/ml) (SouthernBiotech) for 20 min.

PMS was prepared as previously described (50). Briefly, 1.5 × 10⁵ 293A cells per well were seeded in the poly-D-lysine-coated wells of an eight-well Lab-Tek chamber (Nunc, #1.5 German glass type) and cultured in a CO₂ cell culture incubator at 37°C for 16 hours.

All the procedure after this point was held at RT. Cells were washed with 1× PMS washing buffer [1× Hanks' balanced salt solution containing 2.5 mM CaCl₂ and 0.5% bovine serum albumin (BSA)], filled the well with the buffer, and sonicated using a small probe-type sonicator with 22% power, 5 s per given area, positioning the probe tip just beneath of the buffer to reveal the inner leaflet of the plasma membrane. After washing with 10 ml of 1× PMS washing buffer to remove all debris and incubating with the blocking buffer (5% BSA-containing 1× PMS buffer) for 30 min, annexin V–biotin (0.5 mg/ml) was added for binding to the PMS for 30 min and washed with 15 ml of 1× washing buffer, and this step was repeated with streptavidin (5 mg/ml) and then 10 nM biotin- and DyLight 650–conjugated goat F(ab')₂ anti-human λ + κ (SouthernBiotech).

BCR signaling assay

To test BCR signaling, 2000 to 3000 sorted B cells were labeled with DyLight 550–conjugated Fab fragments from Jackson Immuno-Research: Goat Anti-Human IgM, Fc5μ fragment specific (10 μg/ml) or Goat Anti-Human IgG, Fcγ fragment specific (10 μg/ml). Cells were dropped in chambers containing PLB–anti-λ/κ and incubated at 37°C for 10 min, followed by fixation with 4% paraformaldehyde. For intracellular pSyk, pBLNK, and pPLC-γ2 staining, cells were permeabilized with 0.1% Triton X-100 for 10 min at RT, followed by overnight staining at 4°C with antibodies against pSyk (pY352), pBLNK (pY84), and pPLC-γ2 (pY759) from BD Biosciences. Images were acquired using the Nikon TIRF microscope system equipped with a CFI HP Apochromat TIRF 100×/1.49 oil objective lens (Nikon), a TIR controlling system, an EMCCD (electron multiplying charge coupled device camera, and 405-, 488-, 561-, and 640-nm laser lines controlled by NIS-Elements (Nikon). MFI values of BCR, pSyk, pBLNK, and pPLC-γ2 within the immune synapse and the Pearson's correlation coefficients of signaling molecules and BCR were calculated from background-subtracted images using MATLAB (MathWorks) software.

Membrane antigen internalization and trafficking into the acidic compartment by flow cytometry

To compare Malian B cells' BCR-mediated antigen capturing and internalization followed by antigen trafficking into the acidic compartment among different subsets, we adopted the assay using PMS-bound anti-λ/κ but flow cytometry–based approach. PMS–anti-λ/κ was prepared as described before in detail (50). For tracking anti-λ/κ in intracellular acidic compartment, 10 nM avidin-pHrodo was additionally added to bind to the biotinylated anti-λ/κ. A total of 1 × 10⁶ Malian PBMCs were added to each well and incubated for given times at 37°C to let the B cells respond to the PMS–anti-λ/κ. After chase, cells were collected by brief pipetting and centrifuging and stained with streptavidin-Alexa488 to detect surface anti-λ/κ. To identify the naïve, classical MBCs, and atypical MBCs, CD19-BV650, CD21-BV421, and CD27-Alexa700 antibodies were added at the same time and analyzed by flow cytometry. Using the condition that B cell–bound antigens were only localized on cell surface by incubating cells with the same biotin- and DyLight 650–conjugated anti-λ/κ in solution on ice, conversion factor between anti-λ/κ and streptavidin was obtained from the equation after plotting MFIs between the Ag–DyLight 650 and streptavidin-Alexa488 as follows

Anti-λ/κ–DyLight 650 (MFI) = $a \times$ streptavidin-Alexa488 (MFI) + y , where a is the conversion factor between Ag–DyLight 650 and streptavidin-Alexa488.

Using this value, the value of surface anti- λ/κ (MFI) after chase for a period of time was derived from the value of streptavidin-Alexa488 (MFI) bound on surface, and the percentage of anti- λ/κ internalization was calculated by DyLight 650 MFI of surface divided by that of total in each sample.

Membrane antigen internalization by confocal microscopy

To analyze the localization of internalized antigen relative to the immune synapse, sorted cells were dropped on PMS-anti- λ/κ -DyLight 550 and incubated at 37°C for 30 and 90 min, followed by fixation with 4% PFA and permeabilization with 0.1% Triton X-100 for 10 min at RT. Cells were stained overnight at 4°C with antibodies against HLA-DR, LAMP-1, and γ -tubulin. Confocal Z-stack images were acquired using a Zeiss 880 confocal microscope equipped with a Plan-Apochromat 63 \times /1.4 Oil DIC M27 objective lens, an Airyscan detector (GaAsP), and 405-, 488-, 561-, and 640-nm laser lines controlled by ZEN software (Carl Zeiss). Images were acquired in Airyscan mode and processed using ZEN (Carl Zeiss) software. The MFI of anti- λ/κ -DyLight 550 within the cell at each Z stack and the Mander's coefficient for 3D colocalization of anti- λ/κ with HLA-DR and LAMP-1 were calculated using MATLAB (MathWorks) software. The polarity index of MTOC localization was calculated by dividing the distance of the MTOCs from the PMS by the orthogonal radius of the cell.

In vitro stimulation of B cell subsets and measurement of IRF4 and IRF8 mRNA expression

To test IRF4 and IRF8 expression, 14,000 to 15,000 sorted B cells were incubated in complete RPMI at 37°C with 5% CO₂ for 24 hours in chambers without any stimulations, or with BCR stimulation with either PLBs containing biotinylated goat F(ab')₂ anti-human $\lambda + \kappa$ (SouthernBiotech) for membrane Ag engagement or 10 nM biotinylated goat F(ab')₂ anti-human $\lambda + \kappa$ (SouthernBiotech) for soluble antigen engagement. The cells stimulated for BCR were supplemented with CpG (ODN2006) (1.25 μ g/ml, Invivogen), IL-2 (50 ng/ml, BioLegend), IL-21 (100 ng/ml, BioLegend), IL-10 (250 ng/ml, BioLegend), and BAFF (100 ng/ml, R&D Systems). Following incubation, cells were lysed, and RNA was extracted using Lysis Solution from the Cells-to-CT 1-Step TaqMan Kit (Invitrogen) following the manufacturer's protocol. Expression of IRF4 and IRF8 in the cell lysates was analyzed by reverse transcription and qRT-PCR.

Reverse transcription and qRT-PCR

Reverse transcription and qRT-PCR were performed on the QuantStudio 6 Real-Time PCR System (Applied Biosystems) using the master mix from the Cells-to-CT 1-Step TaqMan Kit (Invitrogen) and the following TaqMan probes from Thermo Fisher Scientific: IRF4 (Hs00180031_m1), IRF8 (Hs00175238_m1), and 18s (Hs03003631_g1). Ct values were calculated using the QuantStudio software. Relative levels of expression of IRF4 and IRF8 mRNA were determined by the $2^{-\Delta\Delta Ct}$ method using 18s as a reference gene for normalization.

Localization of CD19 and Fc γ RIIB in the immune synapse

To determine the localization of CD19 and Fc γ RIIB in the immune synapse, 2000 to 3000 sorted B cells were labeled with Alexa Fluor 488-conjugated Fab fragments of anti-CD19 antibodies and DyLight 550-conjugated Fab fragments from Jackson ImmunoResearch: Goat Anti-Human IgM, Fc5 μ fragment specific (10 μ g/ml) or Goat

Anti-Human IgG, Fc γ fragment specific (10 μ g/ml). Cells were dropped in chambers containing PLB-anti- λ/κ and incubated at 37°C for 1, 2, and 10 min, followed by fixation with 4% PFA. Cells were stained with primary antibodies specific for Fc γ RIIB (7D5, Creative Diagnostics), followed by Alexa Fluor 647-labeled Ig-specific secondary antibodies (ThermoFisher). Images were acquired using the Nikon TIRF microscope system equipped with the CFI HP Apochromat TIRF 100 \times /1.49 oil objective lens (Nikon), a TIR controlling system, an EMCCD camera, and 405-, 488-, 561-, and 640-nm laser lines controlled by NIS-Elements (Nikon). MFI values of BCR, CD19, and Fc γ RIIB within the immune synapse and the Pearson's correlation coefficients of BCR and CD19 or Fc γ RIIB were calculated from background-subtracted images using MATLAB (MathWorks) software. The distribution of BCR, CD19, and Fc γ RIIB in the immune synapse was quantified using Fiji (NIH), where an ROI was defined that encompassed the center of the cell with the highest BCR accumulation (Fig. 5B). The MFI in the ROI in the center and outside the ROI in the periphery was measured, and a ratio of MFI (center):MFI (periphery) was calculated.

SUPPLEMENTARY MATERIALS

Supplementary material for this article is available at <http://advances.sciencemag.org/cgi/content/full/6/30/eaba6493/DC1>

[View/request a protocol for this paper from Bio-protocol.](#)

REFERENCES AND NOTES

- World Health Organization, *World Malaria Report 2018* (World Health Organization, Geneva, Switzerland, 2018), 165 pp.
- J. Langhorne, F. M. Ndungu, A.-M. Sponaas, K. Marsh, Immunity to malaria: More questions than answers. *Nat. Immunol.* **9**, 725–732 (2008).
- P. D. Crompton, J. Moebius, S. Portugal, M. Waisberg, G. Hart, L. S. Garver, L. H. Miller, C. Barillas-Mury, S. K. Pierce, Malaria immunity in man and mosquito: Insights into unsolved mysteries of a deadly infectious disease. *Annu. Rev. Immunol.* **32**, 157–187 (2014).
- G. E. Weiss, B. Traore, K. Kayentao, A. Ongoiba, S. Doumbo, D. Doumtabe, Y. Kone, S. Dia, A. Guindo, A. Traore, C.-Y. Huang, K. Miura, M. Mircetic, S. Li, A. Baughman, D. L. Narum, L. H. Miller, O. K. Doumbo, S. K. Pierce, P. D. Crompton, The Plasmodium falciparum-specific human memory B cell compartment expands gradually with repeated malaria infections. *PLoS Pathog.* **6**, e1000912 (2010).
- T. M. Tran, S. Li, S. Doumbo, D. Doumtabe, C. Y. Huang, S. Dia, A. Bathily, J. Sangala, Y. Kone, A. Traore, M. Niangaly, C. Dara, K. Kayentao, A. Ongoiba, O. K. Doumbo, B. Traore, P. D. Crompton, An intensive longitudinal cohort study of malian children and adults reveals no evidence of acquired immunity to Plasmodium falciparum infection. *Clin. Infect. Dis.* **57**, 40–47 (2013).
- G. E. Weiss, P. D. Crompton, S. Li, L. A. Walsh, S. Moir, B. Traore, K. Kayentao, A. Ongoiba, O. K. Doumbo, S. K. Pierce, Atypical memory B cells are greatly expanded in individuals living in a malaria-endemic area. *J. Immunol.* **183**, 2176–2182 (2009).
- P. Holla, A. Ambegaonkar, H. Sohn, S. K. Pierce, Exhaustion may not be in the human B cell vocabulary, at least not in malaria. *Immunol. Rev.* **292**, 139–148 (2019).
- G. R. A. Ehrhardt, J. T. Hsu, L. Gartland, C.-M. Leu, S. Zhang, R. S. Davis, M. D. Cooper, Expression of the immunoregulatory molecule FcRH4 defines a distinctive tissue-based population of memory B cells. *J. Exp. Med.* **202**, 783–791 (2005).
- S. Moir, J. Ho, A. Malaspina, W. Wang, A. C. DiPoto, M. A. O'Shea, G. Roby, S. Kottlilil, J. Arthos, M. A. Proschian, T.-W. Chun, A. S. Fauci, Evidence for HIV-associated B cell exhaustion in a dysfunctional memory B cell compartment in HIV-infected viremic individuals. *J. Exp. Med.* **205**, 1797–1805 (2008).
- S. Portugal, N. Obeng-Adjiei, S. Moir, P. D. Crompton, S. K. Pierce, Atypical memory B cells in human chronic infectious diseases: An interim report. *Cell. Immunol.* **321**, 18–25 (2017).
- S. Wang, J. Wang, V. Kumar, J. L. Karnell, B. Naiman, P. S. Gross, S. Rahman, K. Zerrouki, R. Hanna, C. Morehouse, N. Holowecyk, H. Liu; Autoimmunity Molecular Medicine Team, Z. Manna, R. Goldbach-Mansky, S. Hasni, R. Siegel, M. Sanjuan, K. Streicher, M. P. Cancro, R. Kolbeck, R. Ettinger, IL-21 drives expansion and plasma cell differentiation of autoreactive CD11c^{hi}T-bet⁺ B cells in SLE. *Nat. Commun.* **9**, 1758 (2018).
- L. C. Menard, S. Habte, W. Gonsiorek, D. Lee, D. Banas, D. A. Holloway, N. Manjarrez-Orduno, M. Cunningham, D. Stetsko, F. Casano, S. Kansal, P. M. Davis, J. Carman, C. K. Zhang, F. Abidi, R. Furie, S. G. Nadler, S. J. Suchard, B cells from African American lupus patients exhibit an activated phenotype. *JCI Insight* **1**, e87310 (2016).

13. A. Arazi, D. A. Rao, C. C. Berthier, A. Davidson, Y. Liu, P. J. Hoover, A. Chicoine, T. M. Eisenhaure, A. H. Jonsson, S. Li, D. J. Lieb, F. Zhang, K. Slowikowski, E. P. Browne, A. Noma, D. Sutherland, S. Steelman, D. E. Smilek, P. Tosta, W. Apruzzese, E. Massarotti, M. Dall'Era, M. Park, D. L. Kamen, R. A. Furie, F. Payan-Schober, W. F. Pendergraft III, E. A. Mc Innis, J. P. Buyon, M. A. Petri, C. Putterman, K. C. Kalunian, E. S. Woodle, J. A. Lederer, D. A. Hildeman, C. Nusbaum, S. Raychaudhuri, M. Kretzler, J. H. Anolik, M. B. Brenner, D. Wofsy, N. Hacohen, B. Diamond; Accelerating Medicines Partnership in SLE network, The immune cell landscape in kidneys of patients with lupus nephritis. *Nat. Immunol.* **20**, 902–914 (2019).
14. E. Zumaquero, S. L. Stone, C. D. Scharer, S. A. Jenks, A. Nellore, B. Mousseau, A. Rosal-Vela, D. Botta, J. E. Bradley, W. Wojciechowski, T. Ptacek, M. I. Danila, J. C. Edberg, S. L. Bridges Jr., R. P. Kimberly, W. W. Chatham, T. R. Schoeb, A. F. Rosenberg, J. M. Boss, I. Sanz, F. E. Lund, IFN γ induces epigenetic programming of human T-bet^{hi} B cells and promotes TLR7/8 and IL-21 induced differentiation. *eLife* **8**, e41641 (2019).
15. S. A. Jenks, K. S. Cashman, E. Zumaquero, U. M. Marigorta, A. V. Patel, X. Wang, D. Tomar, M. C. Woodruff, Z. Simon, R. Bugrovsky, E. L. Blalock, C. D. Scharer, C. M. Tipton, C. Wei, S. S. Lim, M. Petri, T. B. Niewold, J. H. Anolik, G. Gibson, F. E.-H. Lee, J. M. Boss, F. E. Lund, I. Sanz, Distinct effector B cells induced by unregulated Toll-like receptor 7 contribute to pathogenic responses in Systemic Lupus Erythematosus. *Immunity* **49**, 725–739.e6 (2018).
16. C. D. Scharer, E. L. Blalock, T. Mi, B. G. Barwick, S. A. Jenks, T. Deguchi, K. S. Cashman, B. E. Neary, D. G. Patterson, S. L. Hicks, A. Khosroshahi, F. E.-H. Lee, C. Wei, I. Sanz, J. M. Boss, Epigenetic programming underpins B cell dysfunction in human SLE. *Nat. Immunol.* **20**, 1071–1082 (2019).
17. C. M. Tipton, C. F. Fucile, J. Darce, A. Chida, T. Ichikawa, I. Gregoret, S. Schieferl, J. Hom, S. Jenks, R. J. Feldman, R. Mehr, C. Wei, F. E.-H. Lee, W. C. Cheung, A. F. Rosenberg, I. Sanz, Diversity, cellular origin and autoreactivity of antibody-secreting cell population expansions in acute systemic lupus erythematosus. *Nat. Immunol.* **16**, 755–765 (2015).
18. S. Portugal, C. M. Tipton, H. Sohn, Y. Kone, J. Wang, S. Li, J. Skinner, K. Virtaneva, D. E. Sturdevant, S. F. Porcella, O. K. Doumbo, S. Doumbo, K. Kayentao, A. Ongoiba, B. Traore, I. Sanz, S. K. Pierce, P. D. Crompton, Malaria-associated atypical memory B cells exhibit markedly reduced B cell receptor signaling and effector function. *eLife* **4**, e07218 (2015).
19. L. Kardava, S. Moir, W. Wang, J. Ho, C. M. Buckner, J. G. Posada, M. A. O'Shea, G. Roby, J. Chen, H. W. Sohn, T.-W. Chun, S. K. Pierce, A. S. Fauci, Attenuation of HIV-associated human B cell exhaustion by siRNA downregulation of inhibitory receptors. *J. Clin. Invest.* **121**, 2614–2624 (2011).
20. F. D. Batista, N. E. Harwood, The who, how and where of antigen presentation to B cells. *Nat. Rev. Immunol.* **9**, 15–27 (2009).
21. B. A. Heesters, C. E. van der Poel, A. Das, M. C. Carroll, Antigen Presentation to B Cells. *Trends Immunol.* **37**, 844–854 (2016).
22. Y. R. Carrasco, F. D. Batista, B cell recognition of membrane-bound antigen: An exquisite way of sensing ligands. *Curr. Opin. Immunol.* **18**, 286–291 (2006).
23. K. Kwak, M. Akkaya, S. K. Pierce, B cell signaling in context. *Nat. Immunol.* **20**, 963–969 (2019).
24. D. Depoil, S. Fleire, B. L. Treanor, M. Weber, N. E. Harwood, K. L. Marchbank, V. L. J. Tymbulewicz, F. D. Batista, CD19 is essential for B cell activation by promoting B cell receptor-antigen microcluster formation in response to membrane-bound ligand. *Nat. Immunol.* **9**, 63–72 (2008).
25. W. Liu, H. Won Sohn, P. Tolar, T. Meckel, S. K. Pierce, Antigen-induced oligomerization of the B cell receptor is an early target of Fc γ R1B inhibition. *J. Immunol.* **184**, 1977–1989 (2010).
26. K. M. Spillane, P. Tolar, B cell antigen extraction is regulated by physical properties of antigen-presenting cells. *J. Cell Biol.* **216**, 217–230 (2017).
27. E. Natkanski, W.-Y. Lee, B. Mistry, A. Casal, J. E. Molloy, P. Tolar, B cells use mechanical energy to discriminate antigen affinities. *Science* **340**, 1587–1590 (2013).
28. M.-I. Yuseff, A. Reversat, D. Lankar, J. Diaz, I. Fanget, P. Pierobon, V. Randrian, N. Larochette, F. Vascotto, C. Desdouets, B. Jauffred, Y. Bellaiche, S. Gasman, F. Darchen, C. Desnos, A. M. Lennon-Duménil, Polarized secretion of lysosomes at the B cell synapse couples antigen extraction to processing and presentation. *Immunity* **35**, 361–374 (2011).
29. U. Klein, S. Casola, G. Cattoretti, Q. Shen, M. Lia, T. Mo, T. Ludwig, K. Rajewsky, R. Dalla-Favera, Transcription factor IRF4 controls plasma cell differentiation and class-switch recombination. *Nat. Immunol.* **7**, 773–782 (2006).
30. H. Xu, V. K. Chaudhri, Z. Wu, K. Biliouris, K. Dienger-Stambaugh, Y. Rochman, H. Singh, Regulation of bifurcating B cell trajectories by mutual antagonism between transcription factors IRF4 and IRF8. *Nat. Immunol.* **16**, 1274–1281 (2015).
31. T. G. Phan, J. A. Green, E. E. Gray, Y. Xu, J. G. Cyster, Immune complex relay by subcapsular sinus macrophages and noncognate B cells drives antibody affinity maturation. *Nat. Immunol.* **10**, 786–793 (2009).
32. K. A. Pape, D. M. Catron, A. A. Itano, M. K. Jenkins, The humoral immune response is initiated in lymph nodes by B cells that acquire soluble antigen directly in the follicles. *Immunity* **26**, 491–502 (2007).
33. R. Roozendaal, T. R. Mempel, L. A. Pitcher, S. F. Gonzalez, A. Verschoor, R. E. Mebius, U. H. von Andrian, M. C. Carroll, Conduits mediate transport of low-molecular-weight antigen to lymph node follicles. *Immunity* **30**, 264–276 (2009).
34. S. F. Gonzalez, L. A. Pitcher, T. Mempel, F. Schuerpf, M. C. Carroll, B cell acquisition of antigen in vivo. *Curr. Opin. Immunol.* **21**, 251–257 (2009).
35. A. A. Ambegaonkar, S. Nagata, S. K. Pierce, H. Sohn, The differentiation in vitro of human tonsil B cells with the phenotypic and functional characteristics of T-bet⁺ atypical memory B cells in malaria. *Front. Immunol.* **10**, 852 (2019).
36. N. Obeng-Adjei, S. Portugal, P. Holla, S. Li, H. Sohn, A. Ambegaonkar, J. Skinner, G. Bowyer, O. K. Doumbo, B. Traore, S. K. Pierce, P. D. Crompton, Malaria-induced interferon- γ drives the expansion of Tbet^{hi} atypical memory B cells. *PLOS Pathog.* **13**, e1006576 (2017).
37. L. Kardava, H. Sohn, C. Youn, J. W. Austin, W. Wang, C. M. Buckner, J. S. Justement, V. A. Melson, G. E. Roth, M. A. Hand, K. R. Gittens, R. W. Kwan, M. C. Sneller, Y. Li, T.-W. Chun, P. D. Sun, S. K. Pierce, S. Moir, IgG3 regulates tissue-like memory B cells in HIV-infected individuals. *Nat. Immunol.* **19**, 1001–1012 (2018).
38. B. Keller, I. Stumpf, V. Strohmeier, S. Usadel, E. Verhoeyen, H. Eibel, K. Warnatz, High SYK expression drives constitutive activation of CD21^{low} B Cells. *J. Immunol.* **198**, 4285–4292 (2017).
39. K. Kwak, N. Quizon, H. Sohn, A. Saniee, J. Manzella-Lapeira, P. Holla, J. Brzostowski, J. Lu, H. Y. Xie, C. Xu, K. M. Spillane, P. Tolar, S. K. Pierce, Intrinsic properties of human germinal center B cells set antigen affinity thresholds. *Sci. Immunol.* **3**, eaau6598 (2018).
40. C. R. Nowosad, K. M. Spillane, P. Tolar, Germinal center B cells recognize antigen through a specialized immune synapse architecture. *Nat. Immunol.* **17**, 870–877 (2016).
41. G. D. Victora, M. C. Nussenzweig, Germinal centers. *Annu. Rev. Immunol.* **30**, 429–457 (2012).
42. M. Fujimoto, Y. Fujimoto, J. C. Poe, P. J. Jansen, C. A. Lowell, A. L. DeFranco, T. F. Tedder, CD19 regulates Src family protein tyrosine kinase activation in B lymphocytes through processive amplification. *Immunity* **13**, 47–57 (2000).
43. D. C. Fong, A. Brauweiler, S. A. Minskoff, P. Bruhns, I. Tamir, I. Mellman, M. Daeron, J. C. Cambier, Mutational analysis reveals multiple distinct sites within Fc γ receptor IIB that function in inhibitory signaling. *J. Immunol.* **165**, 4453–4462 (2000).
44. L. Xu, G. Li, J. Wang, Y. Fan, Z. Wan, S. Zhang, S. Shaheen, J. Li, L. Wang, C. Yue, Y. Zhao, F. Wang, J. Brzostowski, Y. H. Chen, W. Zheng, W. Liu, Through an ITIM-independent mechanism the Fc γ R1B blocks B cell activation by disrupting the colocalized microclustering of the B cell receptor and CD19. *J. Immunol.* **192**, 5179–5191 (2014).
45. H. Fukuyama, F. Nimmerjahn, J. V. Ravetch, The inhibitory Fc γ receptor modulates autoimmunity by limiting the accumulation of immunoglobulin G⁺ anti-DNA plasma cells. *Nat. Immunol.* **6**, 99–106 (2005).
46. J. L. Karnell, N. Dimasi, F. G. Karnell III, R. Fleming, E. Kuta, M. Wilson, H. Wu, C. Gao, R. Herbst, R. Ettinger, CD19 and CD32b differentially regulate human B cell responsiveness. *J. Immunol.* **192**, 1480–1490 (2014).
47. Z. Xiang, A. J. Cutler, R. J. Brownlie, K. Fairfax, K. E. Lawlor, E. Severinson, E. U. Walker, R. A. Manz, D. M. Tarlinton, K. G. C. Smith, Fc γ R1B controls bone marrow plasma cell persistence and apoptosis. *Nat. Immunol.* **8**, 419–429 (2007).
48. M. F. Muellenbeck, B. Ueberheide, B. Amulic, A. Epp, D. Fenyo, C. E. Busse, M. Esen, M. Theisen, B. Mordmüller, H. Wardemann, Atypical and classical memory B cells produce Plasmodium falciparum neutralizing antibodies. *J. Exp. Med.* **210**, 389–399 (2013).
49. H. W. Sohn, P. Tolar, J. Brzostowski, S. K. Pierce, A method for analyzing protein-protein interactions in the plasma membrane of live B cells by fluorescence resonance energy transfer imaging as acquired by total internal reflection fluorescence microscopy. *Methods Mol. Biol.* **591**, 159–183 (2010).
50. C. R. Nowosad, P. Tolar, Plasma membrane sheets for studies of B cell antigen internalization from immune synapses. *Methods Mol. Biol.* **1584**, 77–88 (2017).

Acknowledgments: We thank P. Crompton (NIAID) for providing the PBMC samples collected from individuals in Mali, the scientific team at University of Sciences, Techniques, and Technologies of Bamako, Mali, and the residents of Kalifabougou, Mali for participating in this study. We also thank the Flow Cytometry Core at NIAID for assistance with flow cytometry and cell sorting. **Funding:** This work was supported by the Intramural Research Program of the NIH, NIAID. **Author contributions:** Conceptualization: S.K.P., H.S., and A.A.A.. Methodology: A.A.A., H.S., and K.K. Investigation: A.A.A., H.S., and K.K. Writing (original draft): A.A.A., S.K.P., and H.S. Software: J.M.-L. Resources: J.B. and J.M.-L. Funding acquisition and supervision: S.K.P. **Competing interests:** The authors declare that they have no competing interests. **Data and materials availability:** All data needed to evaluate the conclusions in the paper are present in the paper and/or the Supplementary Materials. Additional data related to this paper may be requested from the authors.

Submitted 19 December 2019
 Accepted 11 June 2020
 Published 24 July 2020
 10.1126/sciadv.aba6493

Citation: A. A. Ambegaonkar, K. Kwak, H. Sohn, J. Manzella-Lapeira, J. Brzostowski, S. K. Pierce, Expression of inhibitory receptors by B cells in chronic human infectious diseases restricts responses to membrane-associated antigens. *Sci. Adv.* **6**, eaba6493 (2020).